Global and Planetary Change 232 (2024) 104328

Contents lists available at ScienceDirect

Global and Planetary Change

journal homepage: www.elsevier.com/locate/gloplacha

Open gridded climate datasets can help investigating the relation between meteorological anomalies and geomorphic hazards in mountainous areas

Roberta Paranunzio [a,*], Francesco Marra [b,c]

[a] Institute of Atmospheric Sciences and Climate, National Research Council of Italy (CNR-ISAC), Torino, Italy
[b] Department of Geosciences, University of Padova, Italy
[c] Institute of Atmospheric Sciences and Climate, National Research Council of Italy (CNR-ISAC), Bologna, Italy

ARTICLE INFO

Editor: Liviu Matenco

Keywords:
Open gridded climate data
Geomorphic hazards
Landslides
Debris flows
Meteorological anomalies
Alps

ABSTRACT

The initiation of geomorphic hazards in mountainous environments is highly susceptible to temperature and precipitation forcing. To assess future changes in these hazards, statistical methods linking meteorological anomalies with the occurrence of past hazards can be employed. These methods are currently trained using long records from in-situ meteorological stations. This requires large efforts for data access, collection and homogenisation, which severely limit the scalability of these approaches. Here, we use a consolidated statistical method and a vast catalogue of geomorphic hazards occurred across the Alpine range to show that open-access datasets of gridded temperature and satellite-based precipitation estimates can be used as surrogates of in-situ observations. Further, we find that satellite data can capture precipitation anomalies leading to debris flows that are missed by in-situ observations.

1. Introduction

The potential impact of climate change on geomorphic hazards in mountainous areas is a major concern for natural systems and society (Hock et al., 2019). In fact, temperature and precipitation are among the main drivers of geomorphic hazards at high-elevations (Chiarle et al., 2021; Guzzetti et al., 2008; Stoffel et al., 2014). Rising air temperatures can destabilise glacierized slopes, as recently seen in the Marmolada disaster of July 2022 (Bondesan and Francese, 2023), as well as non-glacierized slopes, by reducing snow and ice cover and degrading permafrost (Beniston et al., 2018; Chiarle et al., 2021). Glacial retreat exposes sediments which could be mobilised by incoming precipitation. Changes in precipitation patterns may alter the frequency of precipitation-induced hazards such as landslides and debris flows (Gariano and Guzzetti, 2016). These concerns are particularly critical at high altitudes because precipitation and temperature are expected to change with rates that depend on elevation (e.g., Pepin et al., 2015; Dimri et al., 2022), because monitoring networks are less dense, and because large uncertainties still characterise the projections of heavy precipitation at the local scales (Coe and Godt, 2012; Guerreiro et al., 2018). This limits our ability to observe and predict changes in the occurrence of geomorphic hazards in mountainous areas.

Large research attention is devoted to the characterization and modelling of the physical conditions leading to the initiation of geomorphic hazards in mountainous areas (Gariano and Guzzetti, 2016; Mostbauer et al., 2018; Prenner et al., 2018; Schneuwly-Bollschweiler and Stoffel, 2012; Stoffel et al., 2014). However, current global earth system models come short at providing accurate information on temperature and precipitation at the scale relevant for many of these hazards, and high-resolution models able to represent these scales are computationally intensive and only provide short simulations for few emission scenarios (Kendon et al., 2017; Fosser et al., 2020). These issues make the use of physical approaches rather uncertain when it comes to future projections (Alvioli et al., 2018; Peres and Cancelliere, 2018; Rianna et al., 2020). Statistical approaches can be used as alternatives. For example, statistical methods were recently proposed to identify relations between temperature and precipitation at multiple scales and the triggering of different mass-wasting processes (Allen and Huggel, 2013; Paranunzio et al., 2019, 2015). These studies point to the possible use of meteorological anomalies calculated with respect to present climate conditions as a tool to identify the likely initiation and/or preparatory phase of geomorphic hazards at high elevations (Bajni et al., 2021; Paranunzio et al., 2016; Savi et al., 2021). In fact, meteorological anomalies are easier to derive from earth system model

* Corresponding author.
E-mail addresses: r.paranunzio@isac.cnr.it (R. Paranunzio), francesco.marra@unipd.it (F. Marra).

https://doi.org/10.1016/j.gloplacha.2023.104328
Received 30 May 2023; Received in revised form 1 December 2023; Accepted 1 December 2023
Available online 7 December 2023

simulations than physical variables, because they are less sensitive to systematic biases and scale mismatch issues. These approaches may thus help us predicting future risks related to geomorphic hazards in high mountains.

Current statistical approaches require accurate catalogues of past hazardous events, sometimes coupled with information on events non-occurrence (Leonarduzzi et al., 2017; Macciotta et al., 2015; Steger et al., 2022), and are usually based on information from meteorological stations located in proximity of each observed hazardous event (Paranunzio et al., 2016). This comes with two important drawbacks. First, collecting in-situ observations can be very demanding. Reference stations with sufficiently long records of precipitation and temperature need to be identified for each event. This is already a challenging task, especially for precipitation monitoring in mountainous areas, given that the Earth's surface is covered by rain gauges unevenly (Kidd et al., 2017). Then, data from each station need to be collected from the responsible authority, quality-controlled, homogenised and stored. On top of this, restrictive policies often impede the sharing of the meteorological databases, making it difficult to compare the results of different methods (e.g., Mazzoglio et al., 2022). Second, when available, in-situ observations at high-elevations are sparse. In particular, rain gauge inter-distances in operational networks are much larger than the typical scales of variability of heavy convective precipitation (Marra et al., 2016; Villarini et al., 2008). This causes rain gauges to underestimate or even completely miss precipitation events that led to the initiation of serious hazards (Nikolopoulos et al., 2015a; Paranunzio et al., 2016). This is less of a problem for temperature, as temperature gradients are rather smooth and information for high-elevations can be interpolated rather accurately using lapse rates. For example, it was shown that at high elevations interpolated gridded temperatures could provide improved information over model reanalyses (Scherrer, 2020). Overall, the use of ground observations strongly limits the possibility to analyse ungauged or sparsely gauged regions, to quickly examine new hazards inventories and extend available inventories, and to compare the results of different methods; in addition, ground precipitation observations can lead to systematic biases in the quantification of the precipitation conditions leading to some geomorphic hazards. These are the gaps we try to address with this study.

Distributed information from quasi-global open-access gridded datasets are now available for both precipitation and temperature. They cover periods of over 20 years, and have already been used in the context of geomorphic hazards initiation (Brunetti et al., 2021; Handwerger et al., 2022; Nikolopoulos et al., 2017; Nissen et al., 2022; Rossi et al., 2017; Schlögel et al., 2020). They may represent an alternative to ground observations in the case of statistical methods based on meteorological anomalies, because these approaches are less affected by systematic estimation errors.

Here, we take advantage of a consolidated statistical approach for the detection of climate-induced geomorphic hazard (Paranunzio et al., 2019, 2016, 2015) and of a vast database of geomorphic hazards occurred at high elevations ($>$ 1500 m a.s.l.) across the Alpine range (Guerini et al., 2021; Paranunzio et al., 2019). We aim at demonstrating the potential of open access gridded datasets as a surrogate for in-situ observations for wide-scale applications in the framework of geomorphic hazards studies in complex and scarcely instrumented mountain terrain regions. Specifically, we investigate whether two commonly used open gridded datasets can be used as a surrogate of ground observations for the detection of meteorological anomalies leading to the initiation of geomorphic hazards at high-elevations. In this framework, we verify whether satellite-based and interpolated estimates can outperform model-based products, ERA5 in our case, in the detection of significant meteorological anomalies and compared them to estimates derived from ground observations. Further, we check whether these datasets can improve the quality of precipitation information in cases in which in-situ measurements fail to detect an anomaly, such as the relevant case of debris flows triggered by small-scale convective systems.

2. Study area

The Italian Alps represent the southernmost portion of the European Alpine chain, which extends from W to E from the Mediterranean Sea (Franco-Italian border) stretching eastward for about 1200 km to Slovenia. The area covered in this study is about 52,000 km^2, which corresponds to approximately 27% of the European Alps, and has an average elevation of 2500 m a.s.l. (Fig. 1). The morphologic and geologic settings strongly influence the proneness of alpine slopes to failure. The tectonic units of the European Alps are composed of four parts: Penninic, Helvetic, Eastern, and Southern Alpine. The western sector tends to be more compressed than the eastern sector due to the collision between the European and African plates. Consequently, the eastern sector has the greatest diameter while the western sector hosts the highest peaks. The Southern Alpine sector is divided by the other three by the Periadriatic (Insubric) lineament. The crystalline basement is overlapped by Permian volcanic rocks and Mesozoic sediments (limestones, dolomites, and volcano-detritic facies). The Periadriatic Fault divides the Southern Alpine from the other three sectors (Dal Piaz et al., 2003). The Dolomites relief is mainly composed by Mesozoic sediments with peaks up to 3400 m a.s.l.. The Western Italian Alps is characterized by Penninic nappes and mainly composed of limestones, gneiss and granites with peaks up to 4800 m a.sl.

From the climatic point of view, the alpine region is characterized by a high variability of temperature and precipitation at local and regional scale (Auer et al., 2007), which are even enhanced in the Italian alpine region, where local atmospheric patterns interact with a highly complex physiography (Nikolopoulos et al., 2015b; Toreti et al., 2013). At the regional scale, the climate regimes of the Eastern and Western Italian Alps differ significantly. The minimum-maximum annual air temperature range in the reference period 1981–2010 is $-3°/5°$ in the Western Alps and $-1°/8°$ in the Eastern Alps, whereas mean annual precipitation is around 1050 and 850 mm respectively.

The glacial and periglacial environment is experiencing an increase in geomorphic hazards, due to cryosphere changes because of air temperature increase (Chiarle et al., 2022), and to an already ongoing enhancement of convective precipitation extremes (Dallan et al., 2022; Libertino et al., 2019). Moreover, many alpine valleys are facing a rapid urbanisation, with increasing development pressure in terms of people and goods transport. To date, the Italian Alps host $>$14 million people and, with about 80 million tourists per year, are among the most visited regions in the world. This leads to an even growing exposure for resident people and tourists to natural hazards.

3. Data

3.1. Events catalogues

We rely on two main catalogues of geomorphic hazardous events:

(1) the catalogue published by Paranunzio et al. (2019), for which in-situ records are available. This dataset is used to compare the results obtained using gridded open datasets with the ones from in-situ observations;
(2) an extended dataset obtained integrating the dataset at (1) with the dataset published in Guerini et al. (2021) and a small catalogue of 30 slope instability events from CNR-IRPI archives (Nigrelli et al., 2023). This dataset, which represents an updated version of the catalogues by Paranunzio et al. (2019) and Guerini et al. (2021), is here analysed using open gridded products only.

The three data sources used for the catalogue at (2) were derived using the same survey methodology and were subjected to the same quality control procedures (Paranunzio et al., 2019). They can be thus considered homogeneous. The original information on event occurrence and location comes from several sources, including regional

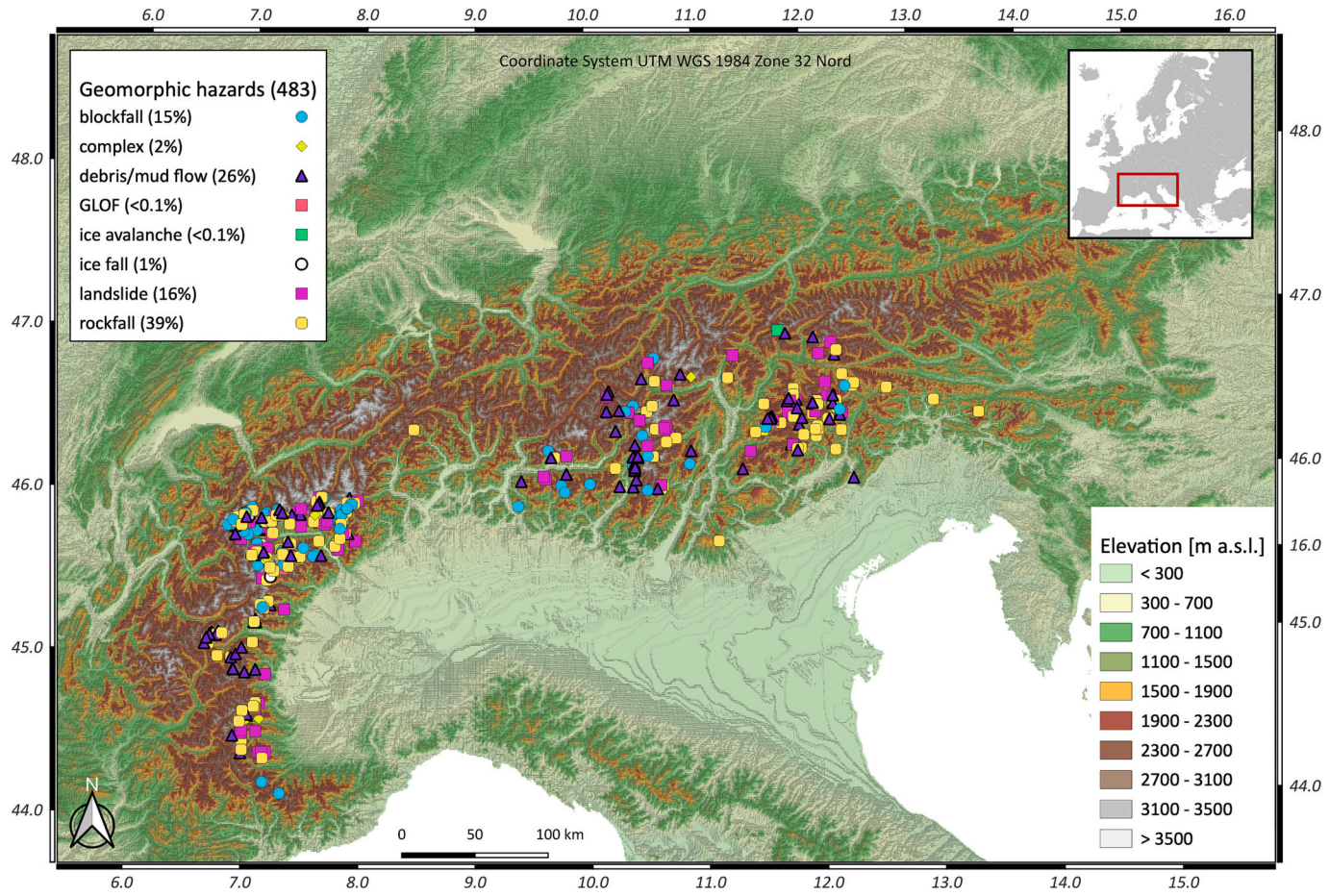

Fig. 1. Study area and location of the 483 events in the catalogue. The events occurred in the Italian Alps in the period 2000–2020 above 1500 m a.s.l.. The percentage of events included in each process typology out of the total has been indicated in the legend. Coordinates are in WGS 84. A modified version of 30-m SRTM DEM of the National Aeronautics and Space Administration (NASA) and the National Imagery and Mapping Agency (NIMA) of the U.S. Department of Defense has been exploited (Farr and Kobrick, 2000).

environmental agencies, journal articles, fire brigade reports, technical documentation of the internal archives of the CNR-IRPI, and newspapers (see Paranunzio et al., 2019 for further details). Events were assigned codes based on the spatial and temporal accuracies. Code 1 means that the initiation area is exact and punctual; 2 is referred to an accurate geolocation of the initiation area (<500 m); 3 is referred to an indicative geolocation of the initiation area (500 m – 2 km). Hazards with lower spatial accuracy is not included in the catalogue. Most of the debris flows are assigned codes 2 and 3, since information on the exact initiation point is not available. In terms of temporal accuracy, code 1 is assigned when the date (and hour occasionally) of the detachment is known, whereas 2 and 3 when the week (or few days period) or only the month (or 30-days period) are known respectively. We limit our analysis to events for which the exact date of occurrence is known at least with temporal accuracy 1 (daily) and spatial accuracy from 1 to 3. Further details on the inclusion criteria of the events in the catalogue are detailed in Paranunzio et al. (2019) and in Guerini et al. (2021).

In total, the dataset at (2) consists of 483 events, of which 358 belong to the dataset (1). These events all occurred in the Italian Alps, above 1500 m a.s.l., in the period 2000–2020 (Fig. 1). The exact type of process was reported wherever available; the dataset includes debris flows (126), rockfalls (190), blockfalls (72), complex landslides (10), ice avalanches (4), ice falls (2), and glacial lake outburst floods (2). When information on the type of process was not available, the slope failure was classified generically as “landslide” (77). For some events, however, the data availability was limited, due to missing values in the ground observations, so that the actual number of events available for analyses of dataset (1) is sometimes lower. It is worth noting that the catalogue is not exhaustive. In fact, the availability of information affects the spatial distribution of the events in the catalogue, especially for remote high-mountain regions where information on slope failures are often incomplete. Moreover, most of the events are reported during summer, due to the higher human presence in these areas during this season. Overall, while we assume that each point in the map corresponds to a single slope failure event, it cannot be excluded that other not-reported events occurred. Nevertheless, our methodological approach does not require the dataset to be complete. It is worth noting that most events have been documented in the last decade with an increasing trend toward 2020.

3.2. *In-situ observations*

In situ-observations of precipitation and temperature are available only for the catalogue in Paranunzio et al. (2019), and are derived from 123 weather stations managed by different local and regional environmental agencies (see details in Paranunzio et al., 2019). Observations were first validated by the responsible agencies and further quality-checked. We use observations of i) daily mean, minimum and maximum 2-m air temperature; ii) daily total precipitation (sum of liquid and solid precipitation). Mean, minimum and maximum temperature over multi-day periods are computed as the average of the respective daily values, while precipitation amounts over multi-day periods are computed as the sum of the daily amounts. In-situ observations are here used as a benchmark to test the ability of the open

gridded datasets to represent the relevant meteorological anomalies. On average, in-situ observations are available for a period of 20 years.

The interested reader can find all the details about the collection and elaboration of in-situ information in Paranunzio et al. (2019).

3.3. Open gridded datasets

We focus here on two open gridded datasets that can be easily accessed by any researcher interested in the topic. We chose observational datasets over high-resolution model reanalyses in order to (a) keep our analyses as much related to observations as possible, (b) avoid potential biases related to model characteristics and performance, and (c) use datasets which are available with homogeneous data handling and format over very large areas. The characteristics of observational datasets are particularly important for the case of convective precipitation, a major trigger of geomorphic hazards, because climate models able to resolve convective processes are not yet vastly available, still do not resolve shallow convection, and cannot properly represent the location and track of convective cells due to the low intrinsic predictability of local-scale atmospheric dynamics (Fosser et al., 2020; Kendon et al., 2021). A comparison with ERA5 has been performed to assess the performance of satellite and interpolated gridded products over model reanalysis in capturing significant meteorological anomalies in the lead-up of the events. Time series of *E*-OBS, IMERG and ERA5 considered in this study cover the period 2000–2020 and thus provide a temporal coverage consistent with the one of in-situ observations.

3.3.1. IMERG

The satellite rainfall dataset considered in this study is the National Aeronautics and Space Administration (NASA)'s Integrated Multi-satellitE Retrievals for GPM (IMERG) version 6 Final Run (Huffman et al., 2020; NASA, 2023a; Tan et al., 2018). IMERG represents the state-of-the-art for what concerns the estimation of precipitation from space and is freely accessible from the NASA data repositories (NASA GES DISC service, NASA, 2023b). It has 0.1° spatial resolution and 30 min temporal resolution with quasi-global coverage (60°S-60°N). The Final Run is released with a latency of a few months. The product combines retrievals from passive microwave and infrared channels, calibrated using the spaceborne radar onboard the GPM core satellites and adjusted using ground observations on a monthly basis. In the last version 6, the IMERG algorithm fuses the early precipitation estimates collected during the operation of the TRMM satellite (2000–2015) with more recent estimates collected during operation of the GPM satellite (2014-present), providing a relatively long record (over 20 years) with homogeneous data processing. IMERG provides precipitation values at a 30-min temporal resolution. In order to get daily resolution comparable to the other datasets, the half-hourly precipitation amounts are summed over 24 h to obtain a daily resolution. As for the case of observations, precipitation amounts over multi-day periods are computed as the sum of these daily amounts.

3.3.2. E-OBS

Interpolated gridded temperature datasets were shown to have lower systematic errors than reanalysis simulations in the representation of air temperature observations in mountainous areas (Scherrer, 2020; Schlögel et al., 2020). Here, we use the E-OBS product. E-OBS was developed specifically for the European domain as part of the European Union Framework 6 ENSEMBLES project (van der Linden and Mitchell, 2009). E-OBS is freely accessible with open licence from the Copernicus Climate Data Store (CDS) (Copernicus Climate Change Service, 2023b). It is a daily gridded observational dataset of precipitation, temperature and sea level pressure. Quality checked station data supplied by national meteorological services were collected within the European Climate Assessment & Dataset (ECA&D) initiative. The temperature in E-OBS is obtained from interpolation of the station values and is provided as an ensemble of equally probable realisations of the variable. A two-stages procedure has been adopted to produce the ensemble of daily fields: first, daily values are fitted with a deterministic model to capture the long-range data spatial trend; then, residuals are interpolated by means of a stochastic method to produce the individual ensemble members. Different methods have been used to incorporate the environmental lapse rate in the last version of the dataset (Cornes et al., 2018). Here, we use the ensemble means of the variable of interest, which represent the best estimate of a given variable.

The full dataset covers the period back to 1950 and provides gridded information on a 0.1° regular grid. Currently, the dataset includes data from 3700 temperature stations, and presents a station density higher than other gridded datasets based on the National Meteorological and Hydrological Services (Cornes et al., 2018), although the number of stations available during a given day may be smaller due to data availability. The number of stations per pixel are irregularly distributed across the continent. Because of its spatial resolution, daily temporal aggregation and temporal coverage, *E*-OBS represents the state-of-the-art for what concerns gridded temperature datasets over Europe, and is particularly suited for climate-induced impact studies such as the one presented here (Nissen et al., 2022; Scherrer, 2020; Van Der Schrier et al., 2013). In this work, daily mean, minimum and maximum air temperature observations have been considered. As for the case of observations, mean, minimum and maximum temperature over multi-day periods are computed as the average of the respective daily values.

3.4. Global reanalysis ERA5

Model reanalyses are largely exploited by the scientific communities to e.g., drive regional climate models, monitor variations in atmospheric patterns and for land applications. With respect to its predecessor ERA-Interim, ERA5 shows a significant improvement in terms of data quality, temporal coverage (1950 to present) and spatio-temporal resolution (0.25°, hourly). ERA5 provides data related to a large number of atmospheric, sea and land-surface states and variables. ERA5 is publicly available online from the CDS (Copernicus Climate Change Service, 2023b). As illustrated in recent studies (Reder and Rianna, 2021), such features make ERA5 suitable for the characterization weather-induced historical events in scarcely instrumented areas, and for operational purposes. In this study, daily 2 m temperature and total precipitation (i.e., the total amount of liquid and frozen water, including rain and snow), are used. As for the case of in-situ observations and satellite estimates, precipitation amounts over multi-day periods are computed as the sum of these daily amounts, while mean temperature over multi-day periods is computed as the average of the respective daily values as for E-OBS.

4. Methods

4.1. Climate data preparation

4.1.1. Selection of the weather station and pixel representative for an event

To identify the most suitable weather stations in the study area, following Paranunzio et al. (2016), we considered (i) the horizontal and altitudinal distance between the initiation area and the weather station, (ii) the temporal coverage of the time series (covering the day of the failure), (iii) similarity of the topographic and climatic contexts. First, we selected weather stations located in the same valley of the initiation area. Second, we relied on stations at a similar altitude and as close as possible to the initiation area. A buffer of 20 km was used to guarantee the climatic representativeness of the failure area (Rianna et al., 2022). Time series with <10 years and discontinuous records were discarded. In case of weather stations reporting only one of the needed variables, different weather stations meeting the criteria were considered for the second variable. This means that, for an individual hazard, precipitation and temperature observations may come from different stations. Gridded products provide rainfall and temperature estimates directly over the initiation area by retrieving the value of the pixel covering the

detachment point.

4.1.2. Identification of the climate variables

We focus on precipitation and temperature examined for the location of the failure (closest station or pixel corresponding to the failure) and aggregated over different time scales, as these variables are (i) easily accessible and often recorded by meteorological agencies, and (ii) they are known to either increase the local susceptibility to the failure (preparatory) or to act as an actual trigger for the failures. Following previous studies based on the same statistical approach (Allen and Huggel, 2013; Paranunzio et al., 2015), we considered mean, minimum and maximum temperature (here denoted as *T*: *T*mean, *T*min, *T*max) at different temporal scales, and precipitation (sum of liquid and solid precipitation, denoted as *R*) accumulated over different temporal aggregations. Temperature and precipitation information are examined over temporal scales of 1 day (the day of the triggering), 7 days (6 days prior to the triggering and the day of the triggering), 30 days (29 days prior and the day of the triggering) and 90 days (89 days prior and the day of the triggering). For *R*, in order to discern the contribute of precipitation on the day of the failure from the one of the antecedent 7 days, an additional 6-day window (i.e., the 6 days prior to the events, excluding the day of the event) has been considered in order to better separate the potential impact of short duration precipitation. In-situ observations are sourced by different local agencies. As such, the raw data availability, also in terms of temporal coverage of the timeseries, depends on the region.

4.2. Identification of the meteorological anomalies

Preparatory factors act on a relatively long temporal scale (days to months) and create conditions that make a possible triggering more likely. Triggering factors act on a short temporal scale and provide the final push needed for the failure to occur. We aim at identifying meteorological anomalies related both to preparatory and triggering factors. To do so, we improve over a consolidated statistical-based approach (Paranunzio et al., 2019, 2016, 2015). The main purpose of this task is to compare the meteorological conditions at the time of the slope failure with the local climatology. We compare easily available (being direct observations and in terms of data availability) climate variables that are expected either to increase the susceptibility to the failure (preparatory) or to be actual triggers. Our target is to identify meteorological anomalies of these variables associated with the initiation of geomorphic hazards. The method is a bottom-up approach i.e., with no a priori information on the events. The main steps are summarised in the subsections below.

4.2.1. Quantification of the meteorological anomaly

The climate variable *V* at the date of the event is compared with a reference sample defined based on the seasonality of the variable. This means that *T* values at the date of the failure are compared with data referring to the same period. Variables referring to intermittent processes, like *R*, are instead compared to a sample including the 45 days before and 45 days after the date of the failure (91 days in total), to extend the reference sample and guarantee robustness of the results. In the case of *R*, days with no precipitation have been removed. Using an empirical cumulative probability distribution $p(V)$, we evaluate whether anomalous conditions of each climatic variable *V* occurred in the lead-up of the slope failures. Specifically, we compute the non-exceedance probability of the value of *V* and we consider it as a meteorological anomaly when $p(V) \leq \alpha/2$ or $p(V) \geq 1-\alpha/2$, being α set at $\alpha = 0.2$. This means that we are in presence of a negative/positive anomaly when $p(V)$ is below/above the 10th/90th percentile. In the case of *R*, a negative anomaly indicates a wet day with amounts of precipitation smaller than the typical climatology. Clearly, such anomalies could be caused by stochastic natural variability. This happens in around 20% of the cases.

4.2.2. Statistical significance of the anomalies

The idea underlying the statistical approach we use (Paranunzio et al., 2019) is that a potential influence of a meteorological variable on the initiation of a geomorphic hazard would manifest as a climatic anomaly, that is an exceedance of a high percentile of the given variable or the non-exceedance of a low percentile. Here, specifically, our aim is to investigate if open gridded datasets could integrate or surrogate in-situ observations in identifying meteorological anomalies. In order to assess whether the meteorological anomalies associated to a given geomorphic hazard are statistically significant, we test them against the null hypothesis of being sampled from a uniform distribution (i.e., only random association between the variable and the hazard). To do so, we use a Monte Carlo approach in which we randomly sample *N* values, where *N* is the number of hazards of a given type, from a uniform distribution (the expected distribution of random percentiles). We compare the number of observed anomalies (i.e., exceedances of the 90th percentile or non-exceedances of the 10th percentile) with the distribution of anomalies obtained from 10^6 replications of the uniform distribution sampling. A number of observed anomalies greater than the 99th percentile of this distribution or smaller than the 1st percentile implies that the likelihood of having the observed anomalies by chance is lower than 1% and is here considered as statistically significant to the level $\alpha = 0.02$.

5. Results

5.1. Extended geomorphic hazard catalogue

The extended catalogue consists of 483 events, and includes rockfalls (190 events), debris/mud flows (126), blockfalls (72), complex landslides (10), ice avalanches (4), glacial lake outburst floods (2), ice falls (2) and more generic landslides that were not associated to any of the above categories (77). Fig. 2 shows the distribution of these events across type of process, season of occurrence and elevation range. As can be seen in Fig. 2a, we observe more events in summer (approximately 45% out of total), followed by spring (32%) and autumn (19.5%). As in Fig. 2b, approximately 56% of the rockfalls occurred in the low-elevation range (1500–2500 a.s.l.) and 39% in the medium range (2500–3500 m a.s.l.). Almost all (94%) debris flows are recorded in the low elevation range, as well as landslides (94%) and blockfalls (74%). To summarize, most rockfalls occur in summer at medium range elevation (39%), whereas spring (33%), autumn (23%) and winter (<5%) rockfalls occur in the lowest range. Similarly, most debris flows occur in summer (approx. 67%), around 20% in spring and 13% in autumn and almost all between 1500 and 2500 a.s.l. Blockfalls are distributed equally between summer and spring (ranging between 36%–38%), whereas landslides are documented mainly in spring (44%) rather than summer (32%) and autumn (17%). Less represented geomorphic hazards like ice-related processes (ice fall and ice avalanche) occur in the 2500–4500 m a.s.l. elevation range, whereas generic landslides events are documented mainly in spring at the lowest elevation range, as well as complex landslides. In the following, we focus on four types of hazards (blockfalls, rockfalls, debris/mudflows, and generic landslides) for which a sufficient sample is available.

5.2. In-situ versus open gridded datasets

We computed the non-exceedance probability $p(V_k)$ associated with the variable *V* of the k^{th} event, $k = 1 \ldots N$ (being *N* the number of events) for the entire catalogue (2). In order to assess the ability of open gridded datasets to represent the distribution of climatic variables associated with geomorphic hazards, we compare the obtained distributions with the ones derived from observations focusing on the catalogue (1), for which in-situ records are available (i.e., in 358 cases out of 483 events) (Fig. 3). The same comparison has been performed between ERA5 data and in-situ records. Following (Paranunzio et al., 2019), we focus on the

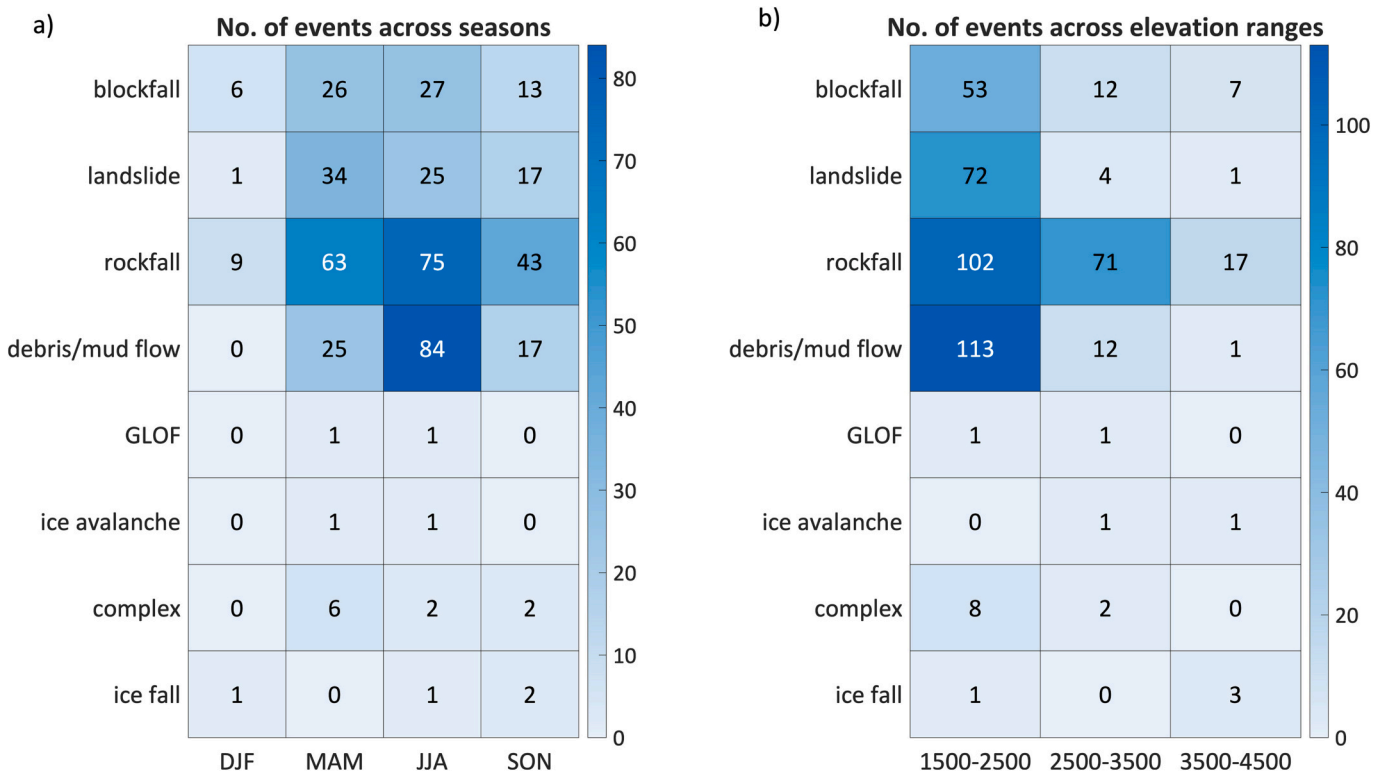

Fig. 2. Spatiotemporal distribution of the geomorphic hazardous events considered in catalogue 2; a) count of events number across type of process and season (DJF: December–January-February, MAM: March–April-May, JJA: June–July-August, SON: September–October-November); b) counts of the events across type of process and elevation range (1500–2500 m a.s.l., 2500–3500 m a.s.l., 3500–4500 m a.s.l.).

temperature variable with the highest availability of data (i.e., *T*mean) as the most representative. This allows us to simplify the problem by reducing the number of representative variables and to minimizing redundancy. As such, in Figs. 3–6, *T*min and *T*max have been omitted; full results are provided in Fig. S1 and Fig. S2 in the Supporting Information.

To verify whether anomalies in a variable *V* related to a specific geomorphic hazard should be associated with random fluctuations rather than meteorological influence, we tested the statistical significance of the observed anomalies. This provides us a *p*-value for the null hypothesis that the examined hazard type is not associated with anomalies in the examined variable. Figs. 3 to 6 show the results for a sample of four *E*-OBS (*T*mean at 1, 7, 30 and 90 day-scale) and five IMERG (*R* at 1,6,7,30 and 90-day scale) variables and nine ERA5 (*T*mean at 1, 7, 30 and 90 day-scale, *R* at 1,6,7,30 and 90-day scale) variables on catalogue (1) and for the extended geomorphic hazard catalogue (2).

Here, we report only types of process for which at least 10 events are available. Some events were discarded due to data unavailability or missing values in the ground observations. The number of anomalies has been reported in the upper and lower part of each boxplot. Statistically significant (significance level $\alpha = 0.02$) positive anomalies are shown in red, negative in blue, and both negative and positive anomalies in green. Results of the comparison between in-situ and gridded-based percentiles for catalogue (1) are in Figs 3 and 4 and commented below.

5.2.1. *Blockfalls*

Blockfalls show different patterns in temperature and rainfall percentiles at 90-days scale. Gridded-based percentiles return respectively negative and positive anomalies where observed percentiles do not detect any significant anomaly. Some divergences are detected for rainfall anomalies at weekly scale (6–7 days). Even if both datasets detect anomalous percentiles, in the case of gridded-based percentiles, the distribution of the values is between the 50th and 99th percentile, differently from observed-based values, meaning that gridded products detected rainfall for which in-situ stations reported almost nothing. This occurs also at daily scale for debris/mud flows and generic landslides.

5.2.2. *Debris/mud flows*

In the specific case of debris flow, significant positive anomalies are reported in observed-based percentiles of *T*mean from 7 to 90-days and *R* at 30 and 90-days scale, which are not detected by gridded products.

5.2.3. *Rockfalls*

Rockfall events show divergences at 7 and 30-days scale in temperature and at 7-days scale in precipitation percentiles. Specifically, observed-based 7 and 30-days *T*mean anomalies are significantly positive differently from gridded-based products. On the other side, in gridded-based analyses significant positive anomalies in rainfall values are detected which are not in the observed ones. ERA5 percentiles of *T*mean disagree with in-situ and *E*-OBS records at daily scale data (Fig. 4).

5.2.4. *Landslides*

Generic landslides show similar patterns in both gridded and observed percentiles. Note that "landslides" includes general processes which have not been classified, although results suggest that they are mainly rainfall-induced. Here, gridded and observed-based percentiles agree. The only exception is represented by daily rainfall. Similar to debris/mud flow events, analyses with satellite products return only positive anomalies, differently from observed-based and ERA5 percentiles which reported both positive and negative (i.e., very small rain amounts) anomalies. ERA5 percentiles do not detect significant positive anomalies in rainfall at weekly and monthly scale, differently from with IMERG and in-situ data (Fig. 4).

In addition, quantile-quantile plots have been performed to compare probability distributions of the observed against gridded-based percen-

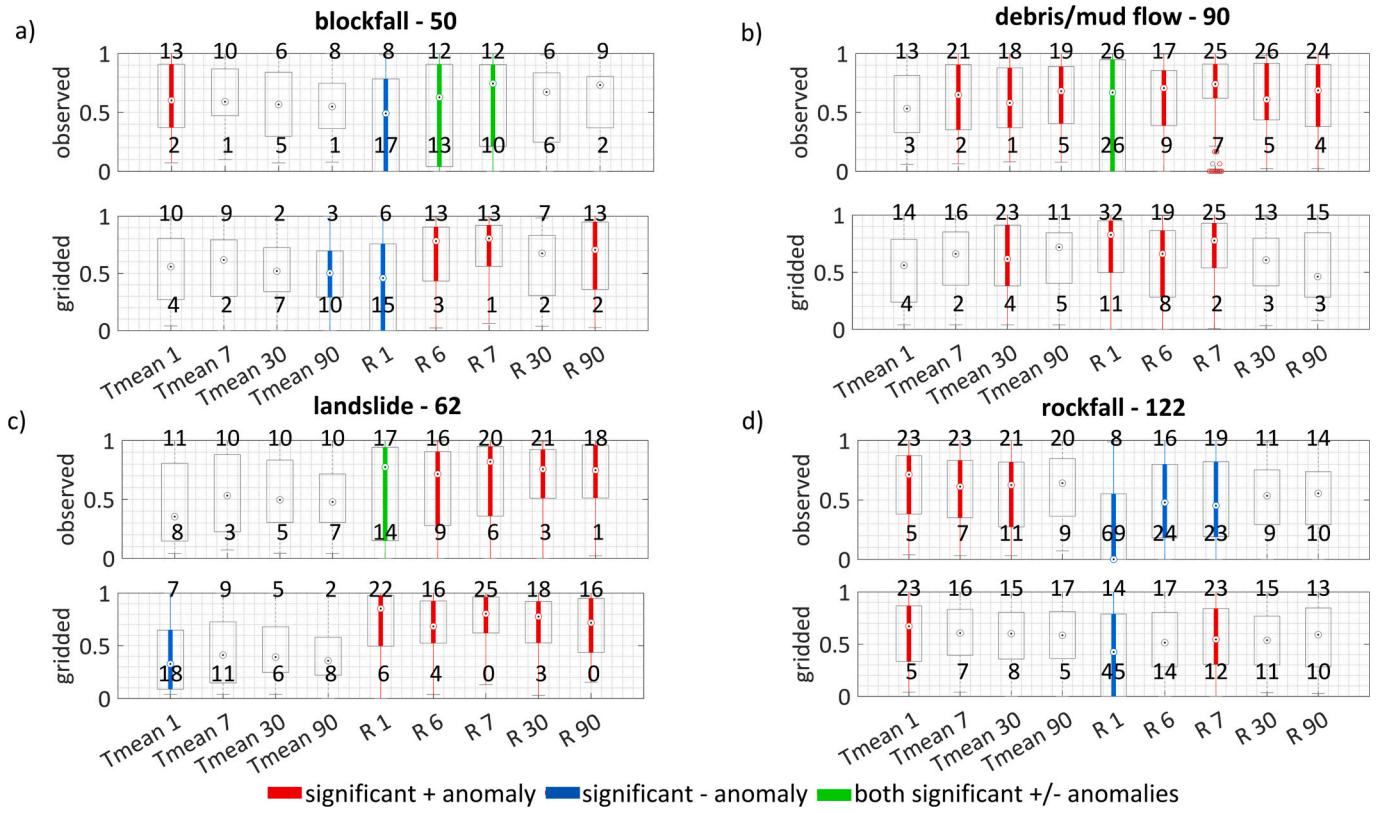

Fig. 3. Boxplots showing the distribution of the percentiles computed for the catalogue 1 for in situ and gridded-based variables (i.e., *E*-OBS and IMERG) across the main typologies of process considered in this study. Red boxplots indicate significant positive (+) anomalies (percentile above or equal to 0.9, 90th percentile), blue boxplots indicate significant negative (−) anomalies (below or equal to 0.1, 10th percentile), green boxplot indicate significant both positive and negative anomalies (+/−) in the considered variables. The numbers above/below the boxplots indicate, for each variable, the number of positive/negative anomalies out of the total number of events (indicated in the boxplot title). (For interpretation of the references to colour in this figure legend, the reader is referred to the web version of this article.)

tiles' distributions for all analysed variables i.e., *T*mean, *T*min, *T*max and *R* (see Figs. S3-S8 in the Supporting Information). This is used as a non-parametric approach to visually assess the similarity of the two underlying distributions. Temperature shows similar patterns across mean, min and max values. In most of the variables, the plot appears linear and close to the $x = y$ line, suggesting that the two samples likely come from the same distribution. Precipitation at 1 and 7 days are skewed (have points far from the diagonal), indicating that one of the distributions has heavier tails than the other one.

When increasing the sample size considerably, as for rockfalls and debris/mud flows events (Fig. 5), the significance of the meteorological anomalies detected by both in-situ and gridded-based records (Fig. 3) is confirmed and, additionally, significant anomalies in additional variables are revealed, while ERA5 data show some differences (see Fig. 6). Temperature anomalies are confirmed to be relevant for rockfalls and statistically significant at all temporal scales, as for debris/mud flows. In the case of landslides, precipitation demonstrates to be crucial over all scales in IMERG-based data while in the ERA5 data the significance is limited to longer-term scales. Here, reanalysis data do not detect any significant anomaly at daily weekly scale indeed. This is still valid for blockfalls, where precipitation anomalies play a role at almost all temporal scales in satellite-based products while reanalyses do not show any significant anomaly (Fig. 6a). Long-term (90 days) temperature anomalies are statistically significant for rockfalls only in the case of *E*-OBS-based percentiles (Fig. 5d). Short-term (1 day) temperature anomaly are significant for landslides and debris/mud flows derived by satellite-based products but not for reanalysis (Figs. 5b and 6b). For such processes, monthly (30 days) and quarterly-scale (90 days) rainfall seem to be no longer significant, as the 90-days temperature anomalies in the case of blockfalls. Analysis performed on *T*min and *T*max confirm these results and reveal additional significant anomalies. This is the case of significant positive anomalies for 7-days *T*min and negative significant anomalies for 1-day *T*max for landslides (see Figs. S1 and S2 in the Supporting Information). As anticipated, the case of debris flows is rather interesting and will be examined in more detail in the following section.

5.3. *The case of debris flows*

Debris/mud flows are related to widespread temperature anomalies at all temporal scales. This is in line with the results of previous works based on ground observations, where temperature was recognized to have a possible role in the initiation and preparation phase (Paranunzio et al., 2019; Ponziani et al., 2020). However, these studies could not find any signal of the impact of daily precipitation on the occurrence of these events. This is unsettling, as water is a necessary ingredient for the triggering of debris flows, and precipitation is the typical source (Guzzetti et al., 2008; Jomelli et al., 2019). As mentioned above, this may be due to the known inability of rain gauges to represent debris-flow triggering rainfall (e.g., Marra et al., 2016; Destro et al., 2017). Indeed, this issue is not present anymore in our results based on satellite precipitation estimates, as these estimates are able to better capture rainfall events with large spatial variability (Marra et al., 2017).

Fig. 7 shows the percentiles of precipitation at daily scale computed by using IMERG against observations. Here we focus on debris/mud flows, which are mainly rainfall-induced processes for which previous studies based on in-situ data showed no significant anomaly in the triggering precipitation (R at 1 day). The figure clearly shows that in

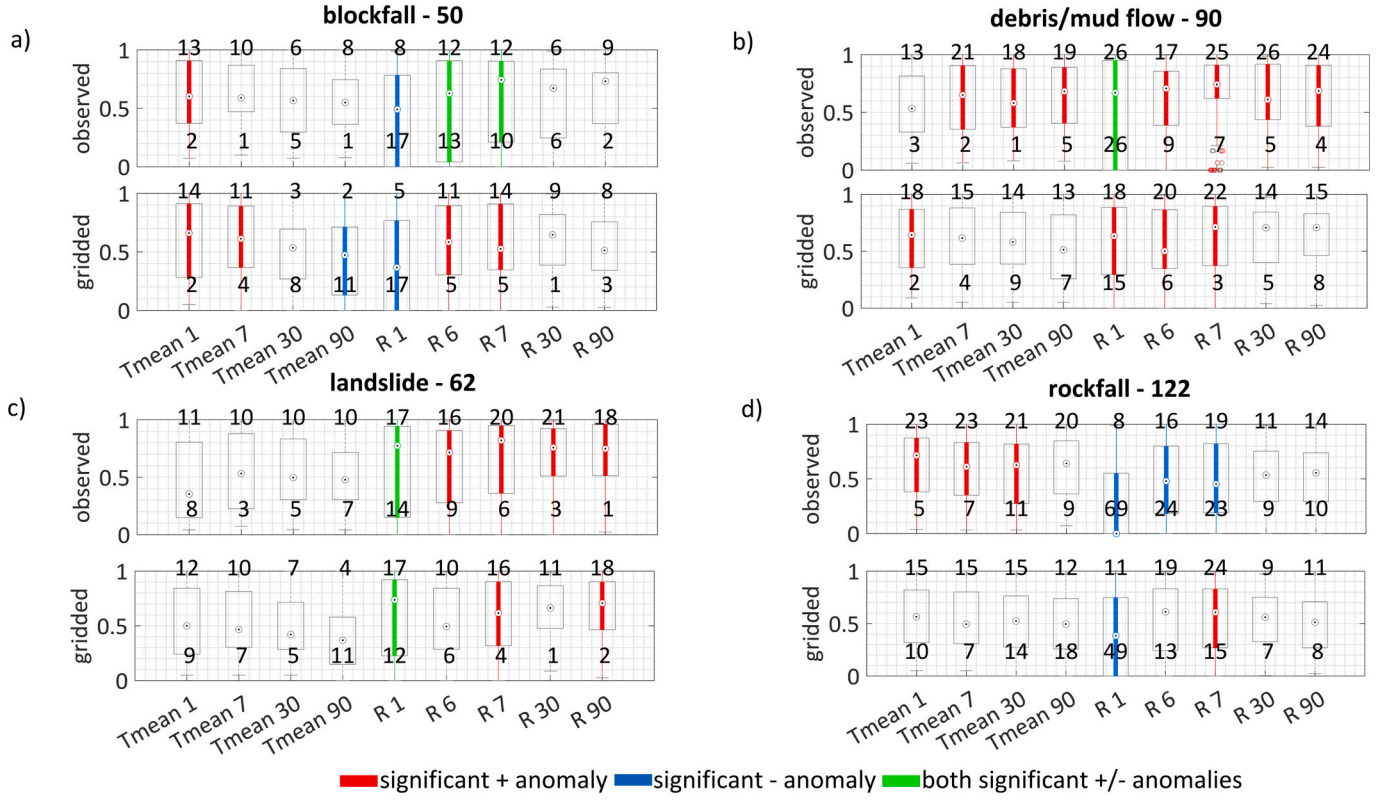

Fig. 4. Boxplots showing the distribution of the percentiles computed for the catalogue 1 for in situ and ERA5 variables across the main typologies of process considered in this study. Red boxplots indicate significant positive (+) anomalies (percentile above or equal to 0.9, 90th percentile), blue boxplots indicate significant negative (−) anomalies (below or equal to 0.1, 10th percentile), green boxplot indicate significant both positive and negative anomalies (+/−) in the considered variables. The numbers above/below the boxplots indicate, for each variable, the number of positive/negative anomalies out of the total number of events (indicated in the boxplot title). (For interpretation of the references to colour in this figure legend, the reader is referred to the web version of this article.)

almost all the cases, IMERG is able to detect precipitation when the stations are not. This is true for all processes, but particularly for debris/mud flows, with a large number of cases in which the precipitation anomaly is >0.9 although the stations observed no precipitation. In just 4 cases IMERG could not detect precipitation that the stations detected, but in none of those, the anomaly was higher than 0.9.

6. Discussion

In this study, we discuss the potential of open gridded climate datasets as a surrogate of ground-based measurements for the detection of meteorological anomalies leading to the initiation of geomorphic hazards in mountainous regions. In the sections below, we discuss the potential of open-access gridded datasets, along with a critical analysis of the major outcomes and insights for future studies.

6.1. *The potential of open gridded meteorological datasets*

The statistical significance of the meteorological anomalies associated with a given geomorphic hazard have been assessed here for the first time. It revealed that some variables are particularly relevant in the initiation/preparation phase of a specific process. While we should keep in mind that statistical significance is not proof of a cause-and-effect relationship, it is important to highlight the importance of this step toward a critical assessment of the possible relations between meteorological anomalies and hazards. We acknowledge that, in a generalized context of climate change and rising temperatures, it is not straightforward to address the physical relation between temperature anomalies and slope failure occurrence. Nevertheless, recent studies agree that neglecting the behavior of such non-ordinary conditions in the triggering/preparatory phase of mass-wasting processes may lead to misleading process interpretation. It is thus crucial to focus future efforts on the most relevant variables and, mostly, temporal scales. To account for this issue, we included only variables for which a physical relationship to slope failure occurrence has already been established in previous studies on the topic.

The quantitative assessment included in this study allowed us to quantitatively compare the results based on ground-based and gridded datasets. In the case of air temperature, some deficiencies between station data and interpolated datasets are revealed when compared to each other. For instance, in-situ stations reveal some significant positive anomalies which interpolated datasets do not reveal. One possible explanation can be the altitude mismatch between the station and the nearest grid point (Krauskopf and Huth, 2020), although the limited (even if relatively large) number of events creates challenges for the assessment of this statistical significance. Moreover, the time-varying number of stations used in the interpolation can introduce an artificial trend (Krauskopf and Huth, 2020). However, the interpolation procedure is beneficial for many reasons, since it provides a more regular and complete coverage of the area of interest and thus a more accurate assessment of temperature anomalies (Cornes et al., 2018; Haylock et al., 2008).

Anomalies missed by local weather stations tend to be associated with local small convective storms characterized by high temporal and spatial variability at sub-daily scale. As demonstrated by Marra et al. (2016), on average, the event-cumulated rainfall field presents a local peak corresponding or close to the debris flow initiation area with rain depth showing a systematic underestimation with the distance, from 70% to 40% at respectively 5 and 10 km distance from the initiation area. This rainfall decay becomes stronger with short-duration rainfall

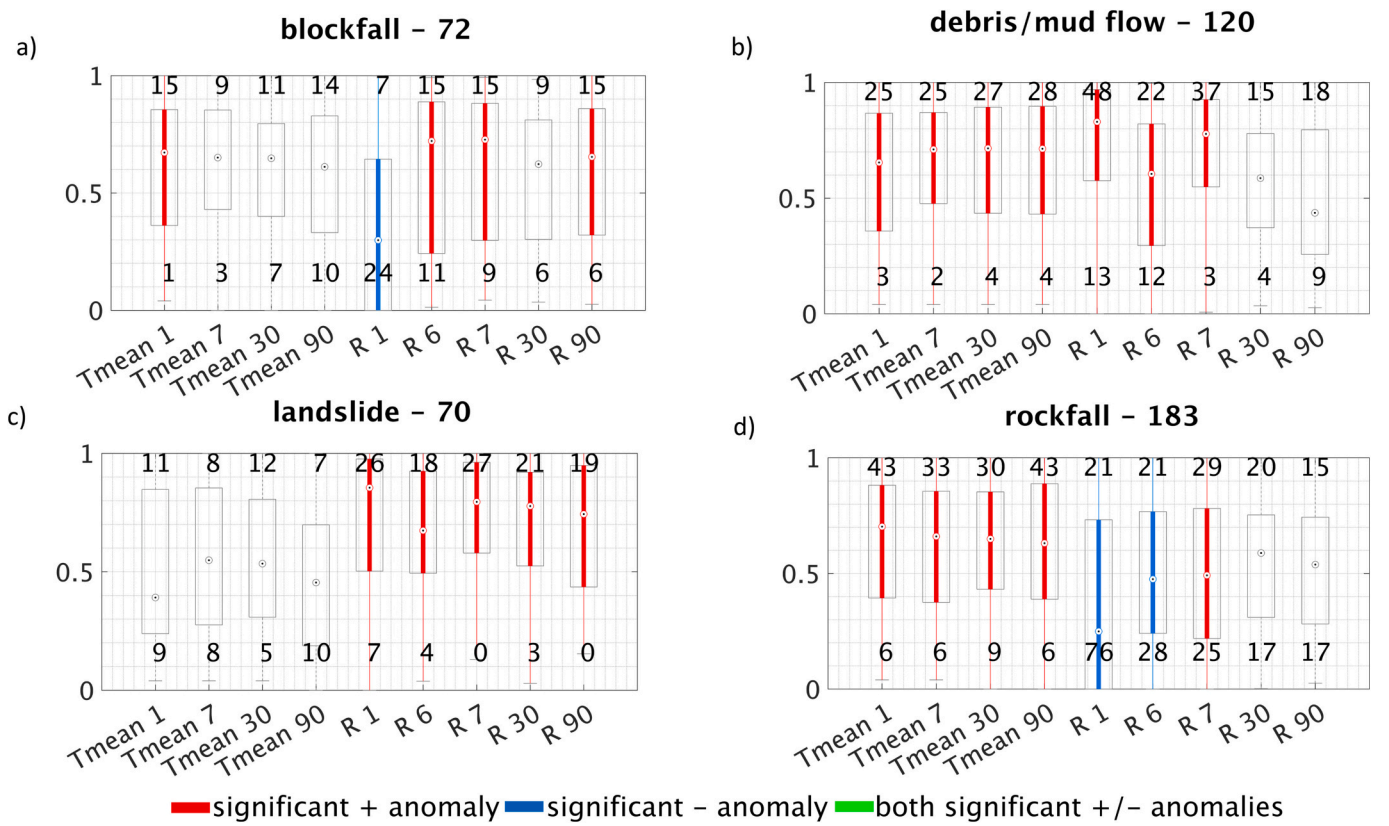

Fig. 5. Boxplots showing the distribution of the percentiles computed for the extended catalogue 2 for gridded-based variables only (i.e., E-OBS and IMERG) across the main typologies of process considered in this study. Red boxplots indicate significant positive (+) anomalies (percentile above or equal to 0.9, 90th percentile), blue boxplots indicate negative (−) anomalies (below or equal to 0.1, 10th percentile), green boxplot indicate both significant positive and anomalies (+/−) in the considered variables. The numbers above/below the boxplots indicate, for each variable, the number of positive/negative anomalies out of the total number of events (indicated in the boxplot title). (For interpretation of the references to colour in this figure legend, the reader is referred to the web version of this article.)

events. This implies that short-duration precipitation events which led to debris flows are affected by larger underestimation when measured away from the initiation area. The results confirm our working hypothesis that satellite estimates can capture precipitation events with high spatial variability at sub-daily scale such as the convective storms typically associated with rainfall-induced events like debris flows and mudflows (Marc et al., 2022). In particular, the ability of satellites to sample the atmosphere in a rather continuous way at a fine spatial and temporal (sub-daily) resolution allows one to detect precipitation anomalies for a number of debris/mud flows events for which in-situ measurements reported no precipitation over the entire day (e.g., see Marra et al., 2017).

So far, satellite-based rainfall estimates have been scarcely exploited for predicting the spatiotemporal occurrence of geomorphic hazards. Some scepticism could be related to e.g., the timeliness and spatiotemporal resolution, which make ground-based measurements always preferred for geomorphic hazards studies instead (Brunetti et al., 2018). But the main issue concerning their use is the relatively low quantitative accuracy. Inaccurate data cannot be used as input of physically-based hydrological and/or geotechnical models, and cannot be used together with other data sources in statistical models such as the one used here. We acknowledge that, when making comparison among climate variables derived from different products, some issue related to the spatial scale mismatch can emerge, due to the different resolution and data source and to the spatiotemporal characteristics of the rainfall events (Brunetti et al., 2018; Marra et al., 2016). Since observations are obtained by point measurements while gridded products provide spatially averaged measurement at the pixel scale, some differences are to be expected. However, quantitative uncertainty is less of a problem for statistical models based on percentiles and anomalies, such as the one used here, since it allows to remove bias in the absolute rainfall estimates and variability among different products (Marc et al., 2022).

We found that ERA5 could reproduce temperature anomalies appropriately, with performance similarly to the one of *E*-OBS. This confirms that modern global reanalysis can reproduce air temperature anomalies satisfactorily, and can be used as an alternative to in-situ observations to detect non-ordinary temperature values, as already reported by previous studies (Schlögel et al., 2020). It is to be noted, however, that recent studies showed that reanalyses may perform worse at reproducing air temperature in winter and at high elevations (Scherrer, 2020). Additionally, the presence of complex terrain (such as in the Alps or mountainous areas in general) could affect the performance of ERA5 (Velikou et al., 2022). This is not particularly problematic for studies focusing on percentile anomalies like this, but caution should be taken when using absolute values of reanalysis-derived air temperatures in remote and scarcely instrumented high-mountain regions.

On the other hand, ERA5 was found to miss several of the significant precipitation anomalies at the weekly scale, especially in the case of mainly rainfall-induced processes like landslides and blockfalls. Conversely, these anomalies could be well detected by IMERG. This is in line with recent studies which suggest that satellite-based products tend to outperform ERA5 model simulations in mountain areas for what concerns the frequency of daily precipitation intensities at the daily scale (Zhou et al., 2023). According to some authors, this is to be ascribed to ERA5 limitations at reproducing the diurnal cycle of precipitation, such as the time of the daily peak or other variations in the magnitude and amplitude of the and diurnal cycle (Lavers et al., 2022). This is related to the resolution of the ERA5 simulations, which does not resolve the convective processes that are critical for heavy precipitation

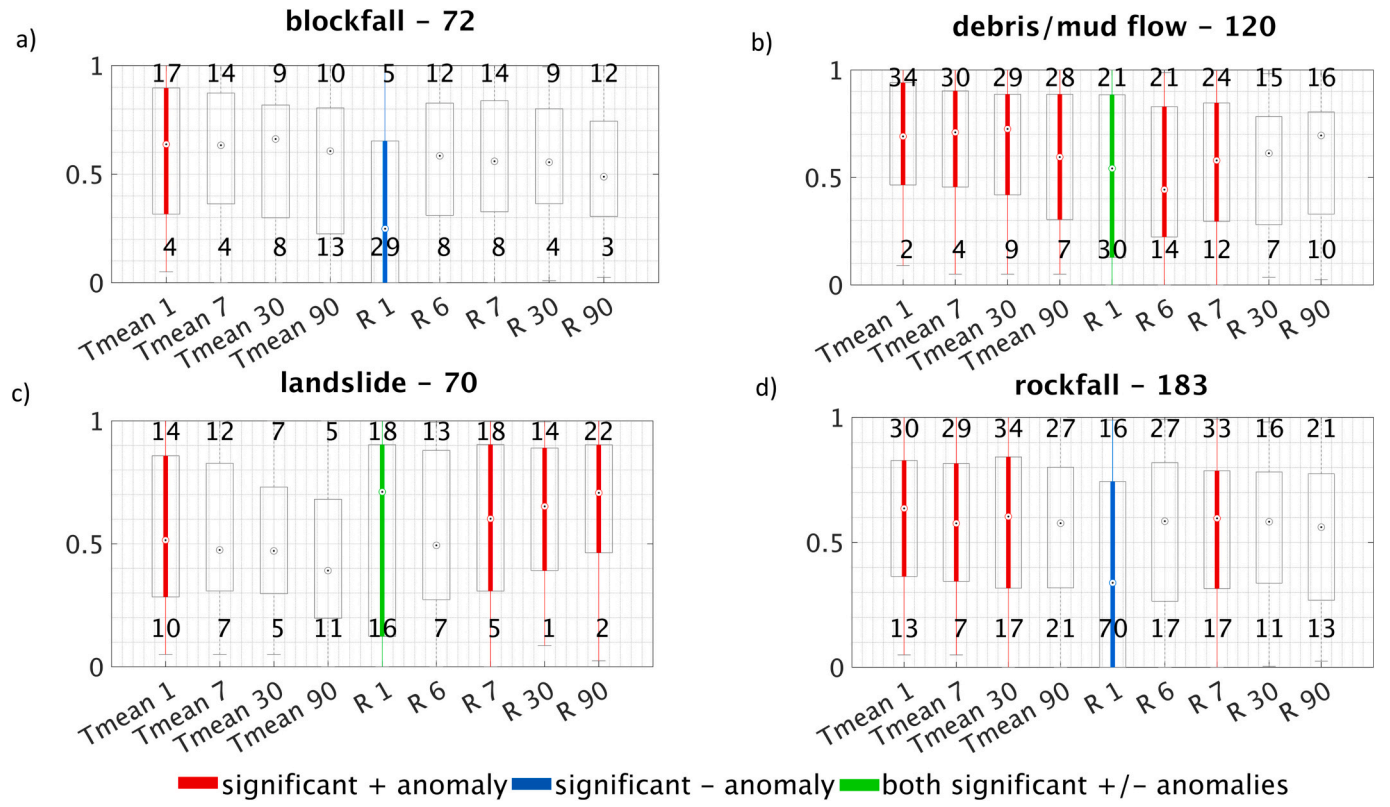

Fig. 6. Boxplots showing the distribution of the percentiles computed for the extended catalogue 2 for ERA5 variables only across the main typologies of process considered in this study. Red boxplots indicate significant positive (+) anomalies (percentile above or equal to 0.9, 90th percentile), blue boxplots indicate negative (−) anomalies (below or equal to 0.1, 10th percentile), green boxplot indicate both significant positive and anomalies (+/−) in the considered variables. The numbers above/below the boxplots indicate, for each variable, the number of positive/negative anomalies out of the total number of events (indicated in the boxplot title). (For interpretation of the references to colour in this figure legend, the reader is referred to the web version of this article.)

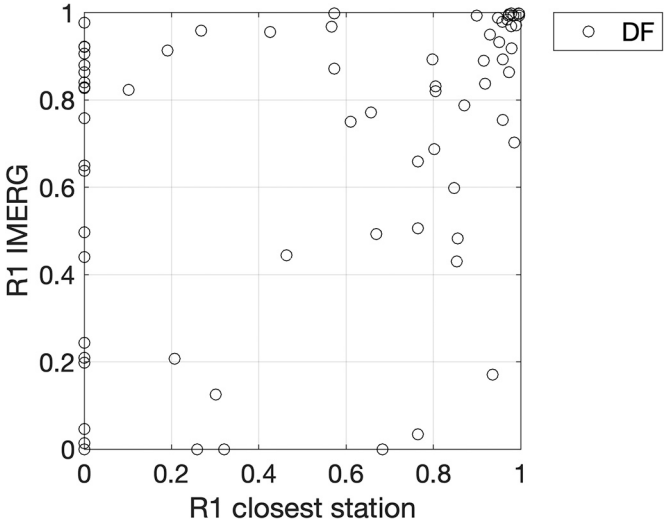

Fig. 7. Percentiles of precipitation at daily scale (R1) computed by employing satellite-based products (IMERG) and in-situ data for debris/mud flows (DF).

at short time scales. Another potential issue is related to the representation of specific precipitation events. Reanalysis and high-resolution models in general, can reproduce the climatology of heavy precipitation relatively accurately (in terms of reproduction of the magnitude, peak time and diurnal cycles variation, Lavers et al., 2022), but fail at reproducing the exact location and track of convective events due to the intrinsic chaotic nature of atmospheric dynamics, and to the large scale-mismatch between the synoptic-scale forcing of extreme events and the local nature of convective processes. This is true even for models running at a convection permitting resolution (e.g., Rinat et al., 2021). Conversely, satellite-based products provide a real-world observational perspective (i.e., an observation of what occurred), although indirect and sometimes inaccurate, and therefore have a relatively good capability to detect location and track of storms even for relatively small-scale precipitation events. In addition to this, satellite-based precipitation products have a uniform data handling and structure, which provide consistent long-term records at the quasi-global scale.

Overall, our results show that IMERG and E-OBS are able to provide information on precipitation and temperature anomalies, respectively, that is comparable to, and in some cases better than, the one provided by in-situ observations and model reanalyses. Open-access gridded datasets can thus be used to complement or replace in-situ data in studies linking meteorological anomalies with the occurrence of geomorphic hazards.

6.2. *Effect of anomalies on the triggering/preparatory phase*

At a regional scale, it is complex to differentiate between triggering and preparatory factors and to clearly identify the main responsible for the failures. This needs to be investigated in the light of the spatial and temporal conditions of the mass wasting processes and along with the geomorphological and lithological context (e.g., Jomelli et al., 2019; Tiranti et al., 2023). Therefore, we focus here on the different categories of hazards in general, with the aim of investigating how gridded datasets may replace or complement in-situ observations.

In the case of rockfalls, temperature anomalies are significant at all the temporal scales. These hazards are strongly temperature-related, as found using in-situ estimates (Paranunzio et al., 2019) and in line with

other studies on the topic (Bajni et al., 2021). High temperatures affect the cryosphere and related slope-stability dynamics by influencing near-surface processes at shorter time scales, and in-depth processes at longer temporal scales, and by enhancing active layer thickening or causing precipitation to fall as rain rather than as snow (Paranunzio et al., 2016). Results highlight that rockfalls occur especially at the highest ranges of elevation in summer and late spring. Gridded estimates confirm that precipitation seems not to be particularly relevant for these processes except for the weekly scale. The increasing susceptibility observed at high altitudes is coherent with the findings of Bajni et al. (2021) and Messenzehl et al. (2017). In particular, the latter speculates that the increasing rockfall frequency could be due to permafrost degradation, causing build-up pressure and water seepage similarly to freeze-thaw cycles leading to rock mass destabilization in depths (D'Amato et al., 2016). According to the summer air temperature trend in the study areas (Nigrelli and Chiarle, 2023), we expect that in the future climate change, by anticipating snow-melting, enhancing thawing of the active layer and glacier shrinkage over time, could make slopes more exposed to instability and these events occur on a longer time period during the year (Bajni et al., 2021; Viani et al., 2020).

A relevant number of occurrences are documented in spring autumn as well. In spring, the major role of precipitation emerges. Events occurred in autumn are characterized by anomalies in temperature at the short-term, in combination or not with precipitation (1 and 7 days), as observed in previous studies (Paranunzio et al., 2019). Recent studies (Haberkorn et al., 2021; Magnin et al., 2015) reported prolonged periods of permafrost active layer thawing in steep alpine rock walls; thawing continues steadily during summer and autumn until reaching its maximum depths in the late autumn, when the ground surface is already in freezing conditions. This situation can favor build-up pressure in the slope up to the failure. The role of temperature is even more evident for winter events, although the relation with short-term temperature anomalies is less clear to explain, also due to the very limited sample size in this season; thus, any outcome should thus be considered carefully. As for autumn events, short-term warm conditions may cause and accelerate snowmelt; this water input could potentially contribute to water-pressure build-up, able to trigger mass-wasting processes on unstable slopes.

Blockfalls and landslides show statistically significant wide-spread precipitation anomalies at all temporal scales. Antecedent precipitation conditions are found to be significantly associated with such geomorphic hazards. They can be considered as a proxy of antecedent soil moisture, which may decrease the amount of shorter-term precipitation needed to trigger shallow landslides (Iverson, 2000).

Debris/mudflows require, by definition, large amounts of water. They are mainly driven by precipitation, even if temperature anomalies look to be significant in their initiation or preparation, as also shown by in-situ based results (Jomelli et al., 2019; Paranunzio et al., 2019). Recent studies confirm the correlation between long-lasting periods of high temperature and debris flow occurrence during the summer months (Ponziani et al., 2023). Both in-situ and gridded data catch a significant precipitation anomaly at daily and weekly scale. The former appears to be uniformly distributed while the latter detect anomalies in a relevant number of cases where weather stations detected no rainfall. Not-ordinary temperature values may be related to enhanced convective activity, with increased rainfall intensities also at high elevations (Molnar et al., 2015). In addition, temperature-related processes like ground-ice/snow melt, frost-weathering permafrost degradation and superficial runoff may contribute to saturate the debris and contribute to make its mobilisation easier (Ponziani et al., 2023; Savi et al., 2021). In fact, debris flow occurrence is not driven only by availability of water, but also of debris from e.g., channel/scarp bed erosion and mass-wasting processes. At high elevation-sites, an important sediment source is represented by postglacial deposits as well (Turconi et al., 2010).

6.3. Incompleteness of the geomorphic hazard catalogues

A common issue that arises when working with geomorphic hazards inventories is the completeness of the catalogues. We acknowledge that the geomorphic events gathered in the catalogue only represent a limited sample of all the hazards that occurred during the analysed time period in the area and that the availability of recorded geomorphic hazards events has been significantly increased in the last years. This bias could affect conclusions in respect of change in natural hazard occurrence with climate change. For this reason, we limited our analysis to the last decades, in which more information and documentation on such events is available. Nevertheless, the methodological approach used here does not require the geomorphic hazard catalogue to be exhaustive in order to detect meteorological anomalies. The procedure adopted to collect data meets reliability and quality requirements (Brunetti et al., 2015; Turconi et al., 2014). In this framework, satellite Earth observation data could represent a good option to complement the information of geomorphic hazard catalogues especially at high-elevation, where the existing inventories are limited (Schlögel et al., 2020). To this end, the temporal resolution of the information on hazards occurrence retrieved by satellite imaging is a major issue in the framework of the analysis included in this study, which needs at least a daily accuracy to be performed. Looking at Fig. 1, it can be seen a non-homogenous geographical distribution of geomorphic hazardous events. This is due, as examples, to the different geomorphological and geological conditions of the Alpine sectors (e.g., different slope steepness and susceptibility), landslide occurrence in highly remote areas (and thus hardly documented), presence/absence of efficient regional databases and portals (providing updated data). In this framework, the use of open climate data can increase the exploitation of fragmented catalogues in remote regions worldwide.

7. Conclusions

We explore the possibility of using open-access gridded datasets of meteorological variables (precipitation and temperature) as a surrogate of in-situ observations to detect meteorological anomalies responsible for the preparation or initiation of geomorphic hazards in high-mountain regions. We base our analysis on a consolidated statistical approach for the detection of meteorological anomalies in the lead up of the initiation of geomorphic hazards and of a vast inventory of geomorphic hazards occurred at high elevation in the Italian Alps. We propose a simple method to quantify the statistical significance of a detected anomaly, and we explore the potential of open gridded datasets to provide improved information on the triggering factors in the case of precipitation-driven hazards such as debris flows and mudflows. Our findings can be summarised in two key points:

- Open gridded datasets represent a valid surrogate for in-situ observations. The statistical significance of the paired gridded and observed-based percentiles is often met, although it is not always guaranteed. The observed mismatches are likely due to sampling limitations, especially in the case of geomorphic hazards with small sample size.
- Satellite estimates are crucial in capturing the triggering precipitation at daily scale in some rainfall-induced processes, and are able to detect anomalies that are not sampled by in-situ observation or model reanalyses. This confirms our working hypothesis, and relates to the ability of satellites to capture precipitation events with high

spatial variability, such as the convective storms typically associated with debris flows and mudflows. Using IMERG, we could detect precipitation anomalies at the daily scale for a number of debris/mud flows for which in-situ measurements reported low precipitation or even no precipitation.

Overall, the information retrieved using gridded datasets can prove valuable for improving our knowledge on the relation between meteorological anomalies and geomorphic hazard initiation. Using open gridded datasets can greatly speed-up data retrieval and analysis, allowing for a greater exploitation of available landslide catalogues. This is relevant for remote and/or scarcely gauged regions where weather stations are lacking or not representative of the triggering area and when in-situ measurements show significant inhomogeneities and gaps. The presented results pave the way to future wide-scale applications, which could help us better understand the relations between meteorological anomalies and associated hazards, and thus derive causative links preparatory and triggering factors and hazards.

CRediT authorship contribution statement

Roberta Paranunzio: Writing – review & editing, Writing – original draft, Visualization, Validation, Methodology, Formal analysis, Data curation, Conceptualization. **Francesco Marra:** Writing – review & editing, Writing – original draft, Visualization, Validation, Methodology, Formal analysis, Data curation, Conceptualization.

Declaration of Competing Interest

None.

Data availability

IMERGv6 data was downloaded from the NASA GES DISC service https://gpm.nasa.gov/node/3328 (NASA, 2023). E-OBS v23.1e was downloaded from https://cds.climate.copernicus.eu/cdsapp#!/dataset/insitu-gridded-observations-europe?tab=overview (Copernicus Climate Change Service, 2023). The dataset "Slope failures at high elevation in the Italian Alps in the period 2000-2020" can be found at PANGAEA https://doi.org/10.1594/PANGAEA.931824, an open-source online data repository hosted at PANGAEA (Guerini et al., 2021). ERA5 data was downloaded from https://cds.climate.copernicus.eu/cdsapp#!/dataset/reanalysis-era5-single-levels?tab=overview (Copernicus Climate Change Service, 2023). The dataset "Catasto delle frane di alta quota nelle Alpi italiane" by Nigrelli et al. (2023) can be found at https://geoclimalp.irpi.cnr.it/catasto-frane-alpi/ (Nigrelli et al., 2023).

Acknowledgments

We thank Dr. Marta Chiarle and Dr. Guido Nigrelli of the National Research Council of Italy - Research Institute for Geo-Hydrological Protection (CNR-IRPI) for providing access to CNR-IRPI archives and landslides catalogues. RP and FM were supported by MIUR (Italian Ministry of Education, Universities and Research) through FOE2019 "Cambiamento climatico: mitigazione del rischio per uno sviluppo sostenibile" project. RP was supported by the SCoRE project, funded by European Commission - H2020-LC-CLA-2018-2019-2020. FM was supported by the CARIPARO Foundation through the Excellence Grant 2021 to the "Resilience" Project. RP and FM were supported by the INTENSE project (raINfall exTremEs and their impacts: from the local to the National ScalE) funded by the European Union - Next Generation EU in the framework of PRIN (Progetti di ricerca di Rilevante Interesse Nazionale) programme of the MUR (Italian Ministry of University and Research) (grant 2022ZC2522).

Appendix A. Supplementary data

Supplementary data to this article can be found online at https://doi.org/10.1016/j.gloplacha.2023.104328.

References

Allen, S., Huggel, C., 2013. Extremely warm temperatures as a potential cause of recent high mountain rockfall. Glob. Planet. Chang. 107, 59–69. https://doi.org/10.1016/J.GLOPLACHA.2013.04.007.

Alvioli, M., Melillo, M., Guzzetti, F., Rossi, M., Palazzi, E., von Hardenberg, J., Brunetti, M.T., Peruccacci, S., 2018. Implications of climate change on landslide hazard in Central Italy. Sci. Total Environ. 630, 1528–1543. https://doi.org/10.1016/j.scitotenv.2018.02.315.

Auer, I., Bohm, R., Jurkovic, A., Lipa, W., Orlik, A., Potzmann, R., Schoner, W., Ungersbock, M., Matulla, C., Briffa, K., Jones, P., Efthymiadis, D., Brunetti, M., Nanni, T., Maugeri, M., Mercalli, L., Mestre, O., Moisselin, J.M., Begert, M., Muller-Westermeier, G., Kveton, V., Bochnicek, O., Stastny, P., Lapin, M., Szalai, S., Szentimrey, T., Cegnar, T., Dolinar, M., Gajic-Capka, M., Zaninovic, K., Majstorovic, Z., Nieplova, E., 2007. HISTALP - historical instrumental climatological surface time series of the Greater Alpine Region. Int. J. Climatol. 27, 17–46. https://doi.org/10.1002/joc.1377.

Bajni, G., Corrado, I., Camera, A.S., Apuani, T., Camera, C.A.S., Apuani, T., 2021. Deciphering meteorological influencing factors for Alpine rockfalls: a case study in Aosta Valley. Landslides 18, 3279–3298. https://doi.org/10.1007/s10346-021-01697-3.

Beniston, M., Farinotti, D., Stoffel, M., Andreassen, L.M., Coppola, E., Eckert, N., Fantini, A., Giacona, F., Hauck, C., Huss, M., Huwald, H., Lehning, M., López-Moreno, J.I., Magnusson, J., Marty, C., Morán-Tejéda, E., Morin, S., Naaim, M., Provenzale, A., Rabatel, A., Six, D., Stötter, J., Strasser, U., Terzago, S., Vincent, C., 2018. The European mountain cryosphere: a review of its current state, trends, and future challenges. Cryosphere 12, 759–794. https://doi.org/10.5194/TC-12-759-2018.

Bondesan, A., Francese, R.G., 2023. The climate-driven disaster of the Marmolada Glacier (Italy). Geomorphology 431, 108687. https://doi.org/10.1016/J.GEOMORPH.2023.108687.

Brunetti, M.T., Peruccacci, S., Antronico, L., Bartolini, D., Deganutti, A.M., Gariano, S.L., Iovine, G., Luciani, S., Luino, F., Melillo, M., Palladino, M.R., Parise, M., Rossi, M., Turconi, L., Vennari, C., Vessia, G., Viero, A., Guzzetti, F., 2015. Catalogue of rainfall events with shallow landslides and new rainfall thresholds in Italy. In: Engineering Geology for Society and Territory - Volume 2. Landslide Processes, pp. 1575–1579. https://doi.org/10.1007/978-3-319-09057-3_280.

Brunetti, M.T., Melillo, M., Peruccacci, S., Ciabatta, L., Brocca, L., 2018. How far are we from the use of satellite rainfall products in landslide forecasting? Remote Sens. Environ. 210, 65–75. https://doi.org/10.1016/j.rse.2018.03.016.

Brunetti, M.T., Melillo, M., Gariano, S.L., Ciabatta, L., Brocca, L., Amarnath, G., Peruccacci, S., 2021. Satellite rainfall products outperform ground observations for landslide prediction in India. Hydrol. Earth Syst. Sci. 25, 3267–3279. https://doi.org/10.5194/hess-25-3267-2021.

Chiarle, M., Geertsema, M., Mortara, G., Clague, J.J., 2021. Relations between climate change and mass movement : Perspectives from the Canadian Cordillera and the European Alps. Glob. Planet. Chang. 202, 103499 https://doi.org/10.1016/j.gloplacha.2021.103499.

Chiarle, M., Viani, C., Mortara, G., Deline, P., Tamburini, A., Nigrelli, G., 2022. Large glacier failures in the Italian Alps over the last 90 years. Geogr. Fis. E Din. Quat. 45, 19–40.

Coe, J.A., Godt, J.W., 2012. Review of approaches for assessing the impact of climate change on landslide hazards. In: Eberhardt, E., Froese, C., Turner, K., Leroueil, S. (Eds.), Landslides and Engineered Slopes, Protecting Society through Improved Understanding: Proceedings of the 11th International and 2nd North American Symposium on Landslides and Engineered Slopes, Banff, Canada, 3–8 June. Reston, VA, pp. 371–377.

Copernicus Climate Change Service, 2023. E-OBS daily gridded Meteorological Data for Europe from 1950 to Present Derived from In-situ Observations [WWW Document]. URL. https://cds.climate.copernicus.eu/cdsapp#!/dataset/insitu-gridded-observations-europe?tab=overview (accessed 5.24.23).

Cornes, R.C., van der Schrier, G., van den Besselaar, E.J.M., Jones, P.D., 2018. An ensemble version of the E-OBS temperature and precipitation data sets. J. Geophys. Res. Atmos. 123, 9391–9409. https://doi.org/10.1029/2017JD028200.

Dal Piaz, G.V., Bistacchi, A., Massironi, M., 2003. Geological outline of the Alps. Episodes 26, 175–180.

Dallan, E., Borga, M., Zaramella, M., Marra, F., 2022. Enhanced summer convection explains observed trends in extreme subdaily precipitation in the Eastern Italian. Alps Geophys. Res. Lett. https://doi.org/10.1029/2021GL096727.

D'Amato, J., Hantz, D., Guerin, A., Jaboyedoff, M., Baillet, L., Mariscal, A., 2016. Influence of meteorological factors on rockfall occurrence in a middle mountain limestone cliff. Nat. Hazards Earth Syst. Sci. 16, 719–735. https://doi.org/10.5194/nhess-16-719-2016.

Destro, E., Marra, F., Nikolopoulos, E.I., Zoccatelli, D., Creutin, J.D., Borga, M., 2017. Spatial estimation of debris flows-triggering rainfall and its dependence on rainfall return period. Geomorphology 278, 269–279. https://doi.org/10.1016/j.geomorph.2016.11.019.

Dimri, A.P., Palazzi, E., Daloz, A.S., 2022. Elevation dependent precipitation and temperature changes over Indian Himalayan region. Clim. Dyn. 59, 1–21. https://doi.org/10.1007/s00382-021-06113-z.
Farr, T.G., Kobrick, M., 2000. Shuttle radar topography mission produces a wealth of data. Eos (Washington. DC) 81, 583–585. https://doi.org/10.1029/EO081I048P00583.
Fosser, G., Kendon, E.J., Stephenson, D., Tucker, S., 2020. Convection-Permitting models offer promise of more certain extreme rainfall projections. Geophys. Res. Lett. 47, 1–9. https://doi.org/10.1029/2020GL088151.
Gariano, S.L., Guzzetti, F., 2016. Landslides in a changing climate. Earth-Sci. Rev. 162, 227–252. https://doi.org/10.1016/j.earscirev.2016.08.011.
Guerini, M., Giardino, M., Paranunzio, R., Nigrelli, G., Turconi, L., Luino, F., Chiarle, M., 2021. Slope Failures at High Elevation in the Italian Alps in the Period 2000–2020. https://doi.org/10.1594/PANGAEA.931824.
Guerreiro, S.B., Fowler, H.J., Barbero, R., Westra, S., Lenderink, G., Blenkinsop, S., Lewis, E., Li, X.-F., 2018. Detection of continental-scale intensification of hourly rainfall extremes. Nat. Clim. Chang. https://doi.org/10.1038/s41558-018-0245-3.
Guzzetti, F., Peruccacci, S., Rossi, M., Stark, C.P., 2008. The rainfall intensity-duration control of shallow landslides and debris flows: an update. Landslides 5, 3–17. https://doi.org/10.1007/s10346-007-0112-1.
Haberkorn, A., Kenner, R., Noetzli, J., Phillips, M., 2021. Changes in ground temperature and dynamics in mountain permafrost in the Swiss Alps. Front. Earth Sci. 9, 1–21. https://doi.org/10.3389/feart.2021.626686.
Handwerger, A.L., Fielding, E.J., Sangha, S.S., Bekaert, D.P.S., 2022. Landslide sensitivity and response to precipitation changes in wet and dry climates. Geophys. Res. Lett. 49 https://doi.org/10.1029/2022GL099499 e2022GL099499.
Haylock, M.R., Hofstra, N., Klein Tank, A.M.G., Klok, E.J., Jones, P.D., New, M., 2008. A European daily high-resolution gridded data set of surface temperature and precipitation for 1950-2006. J. Geophys. Res. Atmos. 113, 1–12. https://doi.org/10.1029/2008JD010201.
Hock, R., Rasul, G., Adler, C., Cáceres, B., Gruber, S., Hirabayashi, Y., Jackson, M., Kääb, A., Kang, S., Kutuzov, S., Milner, A., Molau, U., Morin, S., Orlove, B., Steltzer, H.I., 2019. Chapter 2: High Mountain areas. IPCC special report on the ocean and cryosphere in a changing climate. IPCC Spec. Rep. Ocean Cryosph. A Chang. Clim. 131–202.
Huffman, G., Bolvin, D., Braithwaite, D., Hsu, K., Joyce, R., Kidd, C., Nelkin, E., Sorooshian, S., Tan, J., Xie, P., 2020. NASA GPM Integrated Multi-satellitE Retrievals for GPM (IMERG) Algorithm Theoretical Basis Document (ATBD) Version 06. Nasa/Gsfc 29.
Iverson, M., 2000. Landslide triggering by rain infiltration • b dO 0 K. J x Sin 36, 1897–1910.
Jomelli, V., Pavlova, I., Giacona, F., Zgheib, T., Eckert, N., Alps, F., 2019. Respective influence of geomorphologic and climate conditions on debris-flow occurrence in the Northern French Alps. Landslides 16, 1871–1883. https://doi.org/10.1007/s10346-019-01195-7.
Kendon, E.J., Ban, N., Roberts, N.M., Fowler, H.J., Roberts, M.J., Chan, S.C., Evans, J.P., Fosser, G., Wilkinson, J.M., 2017. Do convection-permitting regional climate models improve projections of future precipitation change? Bull. Am. Meteorol. Soc. 98, 79–93. https://doi.org/10.1175/BAMS-D-15-0004.1.
Kendon, E.J., Prein, A.F., Senior, C.A., Stirling, A., 2021. Challenges and outlook for convection-permitting climate modelling. Philos. Trans. R. Soc. A Math. Phys. Eng. Sci. 379 https://doi.org/10.1098/rsta.2019.0547.
Kidd, C., Becker, A., Huffman, G.J., Muller, C.L., Joe, P., Skofronick-Jackson, G., Kirschbaum, D.B., 2017. So, how much of the Earth's surface is covered by rain gauges? Bull. Am. Meteorol. Soc. 98, 69–78. https://doi.org/10.1175/BAMS-D-14-00283.1.
Krauskopf, T., Huth, R., 2020. Temperature trends in Europe: comparison of different data sources. Theor. Appl. Climatol. 139, 1305–1316. https://doi.org/10.1007/s00704-019-03038-w.
Lavers, D.A., Simmons, A., Vamborg, F., Rodwell, M.J., 2022. An evaluation of ERA5 precipitation for climate monitoring. Q. J. R. Meteorol. Soc. 148, 3152–3165. https://doi.org/10.1002/qj.4351.
Leonarduzzi, E., Molnar, P., McArdell, B.W., 2017. Predictive performance of rainfall thresholds for shallow landslides in Switzerland from gridded daily data. Water Resour. Res. 53, 6612–6625. https://doi.org/10.1002/2017WR021044.
Libertino, A., Ganora, D., Claps, P., 2019. Evidence for increasing rainfall extremes remains elusive at large spatial scales: the case of Italy. Geophys. Res. Lett. 49 https://doi.org/10.1029/2019GL083371.
van der Linden, P., Mitchell, J.F.B., 2009. ENSEMBLES: Climate Change and its Impacts: Summary of Research and Results from the ENSEMBLES Project. Exeter EX1 3PB, UK.
Macciotta, R., Martin, C.D., Edwards, T., Cruden, D.M., Keegan, T., 2015. Quantifying weather conditions for rock fall hazard management. Georisk Assess. Manag. Risk Eng. Syst. Geohazards 11, 272–284. https://doi.org/10.1080/17499518.2015.1061673.
Magnin, F., Deline, P., Ravanel, L., Noetzli, J., Pogliotti, P., 2015. Thermal characteristics of permafrost in the steep alpine rock walls of the Aiguille du Midi (Mont Blanc Massif, 3842 m a.s.l). Cryosphere 9, 109–121. https://doi.org/10.5194/tc-9-109-2015.
Marc, O., Jucá Oliveira, R.A., Gosset, M., Emberson, R., Malet, J.P., 2022. Global assessment of the capability of satellite precipitation products to retrieve landslide-triggering extreme rainfall events. Earth Interact. 26, 122–138. https://doi.org/10.1175/EI-D-21-0022.1.
Marra, F., Nikolopoulos, E.I., Creutin, J.D., Borga, M., 2016. Space–time organization of debris flows-triggering rainfall and its effect on the identification of the rainfall threshold relationship. J. Hydrol. 541, 246–255. https://doi.org/10.1016/j.jhydrol.2015.10.010.
Marra, F., Destro, E., Nikolopoulos, E.I., Zoccatelli, D., Dominique Creutin, J., Guzzetti, F., Borga, M., 2017. Impact of rainfall spatial aggregation on the identification of debris flow occurrence thresholds. Hydrol. Earth Syst. Sci. 21, 4525–4532. https://doi.org/10.5194/hess-21-4525-2017.
Mazzoglio, P., Butera, I., Alvioli, M., Claps, P., 2022. The role of morphology in the spatial distribution of short-duration rainfall extremes in Italy. Hydrol. Earth Syst. Sci. 26, 1659–1672. https://doi.org/10.5194/HESS-26-1659-2022.
Messenzehl, K., Meyer, H., Otto, J.-C., Hoffmann, T., Dikau, R., 2017. Regional-scale controls on the spatial activity of rockfalls (Turtmann Valley, Swiss Alps) — a multivariate modeling approach. Geomorphology 287, 29–45. https://doi.org/10.1016/J.GEOMORPH.2016.01.008.
Molnar, P., Fatichi, S., Gaál, L., Szolgay, J., Burlando, P., 2015. Storm type effects on super Clausius-Clapeyron scaling of intense rainstorm properties with air temperature. Hydrol. Earth Syst. Sci. 19, 1753–1766. https://doi.org/10.5194/HESS-19-1753-2015.
Mostbauer, K., Kaitna, R., Prenner, D., Hrachowitz, M., 2018. The temporally varying roles of rainfall, snowmelt and soil moisture for debris flow initiation in a snow-dominated system. Hydrol. Earth Syst. Sci. 22, 3493–3513. https://doi.org/10.5194/hess-22-3493-2018.
NASA, 2023a. IMERG: Integrated Multi-satellitE Retrievals for GPM|NASA Global Precipitation Measurement Mission [WWW Document]. URL. https://gpm.nasa.gov/data/imerg (accessed 5.23.23).
NASA, 2023b. GES DISC [WWW Document]. URL. https://gpm.nasa.gov/node/3328 (accessed 5.23.23).
Nigrelli, G., Chiarle, M., 2023. 1991–2020 climate normal in the European Alps: focus on high-elevation environments. J. Mt. Sci. 20, 2149–2163. https://doi.org/10.1007/s11629-023-7951-7.
Nigrelli, G., Luino, F., Turconi, L., Guerini, M., Giardino, M., Mortara, G., Chiarle, M., 2023. Catasto Delle Frane di Alta Quota Nelle Alpi ITALIANE [WWW Document]. URL. https://geoclimalp.irpi.cnr.it/catasto-frane-alpi/ (accessed 5.23.23).
Nikolopoulos, E.I., Borga, M., Creutin, J.D., Marra, F., 2015a. Estimation of debris flow triggering rainfall: influence of rain gauge density and interpolation methods. Geomorphology 243, 40–50. https://doi.org/10.1016/j.geomorph.2015.04.028.
Nikolopoulos, E.I., Borga, M., Marra, F., Crema, S., Marchi, L., 2015b. Debris flows in the eastern Itlian Alps: seasonality and atmospheric circulation patterns. Nat. Hazards Earth Syst. Sci. 15 https://doi.org/10.5194/nhess-15-647-2015.
Nikolopoulos, E.I., Destro, E., Maggioni, V., Marra, F., Borga, M., 2017. Satellite rainfall estimates for debris flow prediction: an evaluation based on rainfall accumulation-duration thresholds. J. Hydrometeorol. 18, 2207–2214. https://doi.org/10.1175/JHM-D-17-0052.1.
Nissen, K.M., Rupp, S., Kreuzer, T.M., Guse, B., Damm, B., Ulbrich, U., 2022. Quantification of meteorological conditions for rockfall triggers in Germany. Nat. Hazards Earth Syst. Sci. 22, 2117–2130. https://doi.org/10.5194/nhess-22-2117-2022.
Paranunzio, R., Laio, F., Nigrelli, G., Chiarle, M., 2015. A method to reveal climatic variables triggering slope failures at high elevation. Nat. Hazards 76, 1039–1061. https://doi.org/10.1007/s11069-014-1532-6.
Paranunzio, R., Laio, F., Chiarle, M., Nigrelli, G., Guzzetti, F., 2016. Climate anomalies associated with the occurrence of rockfalls at high-elevation in the Italian Alps. Nat. Hazards Earth Syst. Sci. 16, 2085–2106. https://doi.org/10.5194/nhess-16-2085-2016.
Paranunzio, R., Chiarle, M., Laio, F., Nigrelli, G., Turconi, L., Luino, F., 2019. New insights in the relation between climate and slope failures at high-elevation sites. Theor. Appl. Climatol. 137, 1765–1784. https://doi.org/10.1007/s00704-018-2673-4.
Pepin, N., Bradley, R.S., Diaz, H.F., Baraer, M., Caceres, E.B., Forsythe, N., Fowler, H., Greenwood, G., Hashmi, M.Z., Liu, X.D., Miller, J.R., Ning, L., Ohmura, A., Palazzi, E., Rangwala, I., Schöner, W., Severskiy, I., Shahgedanova, M., Wang, M.B., Williamson, S.N., Yang, D.Q., 2015. Elevation-dependent Warming in Mountain Regions of the World. https://doi.org/10.1038/NCLIMATE2563.
Peres, D.J., Cancelliere, A., 2018. Modeling Impacts of Climate chAnge on Return Period of Landslide Triggering. https://doi.org/10.1016/j.jhydrol.2018.10.036.
Ponziani, M., Pogliotti, P., Stevenin, Hervé, Sara Ratto, M., 2020. Debris-flow Indicator for an Early Warning System in the Aosta Valley Region, vol. 104, pp. 1819–1839. https://doi.org/10.1007/s11069-020-04249-5.
Ponziani, M., Ponziani, D., Giorgi, A., Stevenin, H., Ratto, S.M., 2023. The use of machine learning techniques for a predictive model of debris flows triggered by short intense rainfall. Nat. Hazards. https://doi.org/10.1007/s11069-023-05853-x.
Prenner, D., Kaitna, R., Mostbauer, K., Hrachowitz, M., 2018. The Value of using Multiple Hydrometeorological Variables to Predict Temporal Debris Flow Susceptibility in an Alpine Environment. Water Resour. Res. 54, 6822–6843. https://doi.org/10.1029/2018WR022985.
Reder, A., Rianna, G., 2021. Exploring ERA5 reanalysis potentialities for supporting landslide investigations: a test case from Campania Region (Southern Italy). Landslides 18, 1909–1924. https://doi.org/10.1007/s10346-020-01610-4.
Rianna, G., Reder, A., Pagano, L., Mercogliano, P., 2020. Assessing future variations in landslide occurrence due to climate changes: insights from an Italian Test Case. Lect. Notes Civ. Eng. 40, 255–264. https://doi.org/10.1007/978-3-030-21359-6_27/FIGURES/4.
Rianna, G., Comegna, L., Reder, A., Urciuoli, G., Picarelli, L., 2022. A simplified procedure to assess the effects of climate change on landslide hazard in a small area of the Southern Apennines in Italy. Nat. Hazards. https://doi.org/10.1007/s11069-022-05656-6.

Rinat, Y., Marra, F., Armon, M., Metzger, A., Levi, Y., Khain, P., Vadislavsky, E., Rosensaft, M., Morin, E., 2021. Hydrometeorological analysis and forecasting of a 3d flash-flood-triggering desert rainstorm. Nat. Hazards Earth Syst. Sci. 21, 917–939. https://doi.org/10.5194/nhess-21-917-2021.

Rossi, M., Luciani, S., Valigi, D., Kirschbaum, D., Brunetti, M.T., Peruccacci, S., Guzzetti, F., 2017. Statistical approaches for the definition of landslide rainfall thresholds and their uncertainty using rain gauge and satellite data. Geomorphology 285, 16–27. https://doi.org/10.1016/j.geomorph.2017.02.001.

Savi, S., Comiti, F., Strecker, M.R., 2021. Pronounced increase in slope instability linked to global warming: a case study from the eastern European Alps. Earth Surf. Process. Landf. 46, 1328–1347. https://doi.org/10.1002/esp.5100.

Scherrer, S.C., 2020. Temperature monitoring in mountain regions using reanalyses: Lessons from the Alps. Environ. Res. Lett. 15, 044005 https://doi.org/10.1088/1748-9326/ab702d.

Schlögel, R., Kofler, C., Gariano, S.L., Van Campenhout, J., Plummer, S., 2020. Changes in climate patterns and their association to natural hazard distribution in South Tyrol (Eastern Italian Alps). Sci. Rep. 10, 1–9. https://doi.org/10.1038/s41598-020-61615-w.

Schneuwly-Bollschweiler, M., Stoffel, M., 2012. Hydrometeorological triggers of periglacial debris flows in the Zermatt valley (Switzerland) since 1864. J. Geophys. Res. Earth Surface 117, 1–12. https://doi.org/10.1029/2011JF002262.

Steger, S., Moreno, M., Crespi, A., Zellner, P.J., Gariano, S.L., Brunetti, M.T., Melillo, M., Peruccacci, S., Marra, F., Kohrs, R., Goetz, J., Mair, V., Pittore, M., 2022. Deciphering seasonal effects of triggering and preparatory precipitation for improved shallow landslide prediction using generalized additive mixed models. Nat. Hazards Earth Syst. Sci. Discuss. 2022, 1–38. https://doi.org/10.5194/nhess-2022-271.

Stoffel, M., Tiranti, D., Huggel, C., 2014. Climate change impacts on mass movements - Case studies from the European Alps. Sci. Total Environ. 493, 1255–1266. https://doi.org/10.1016/j.scitotenv.2014.02.102.

Tan, J., Huffman, G.J., Bolvin, D.T., Nelkin, E., Tan, J., Huffman, G.J., Bolvin, D.T., Nelkin, E., 2018. The New IMERG V06: improvements and evaluation. AGUFM 2018, H41H–20.

Tiranti, D., Mallen, L., Nicolò, G., 2023. Rockfall hazard estimation and related applications for a preliminary risk assessment at regional scale: an example from northwestern Italian Alps. Landslides. https://doi.org/10.1007/s10346-023-02060-4.

Toreti, A., Schneuwly-Bollschweiler, M., Stoffel, M., Luterbacher, J., 2013. Atmospheric forcing of debris flows in the Southern Swiss Alps. J. Appl. Meteorol. Climatol. 52, 1554–1560. https://doi.org/10.1175/JAMC-D-13-077.1.

Turconi, L., Kumar De, S., Tropeano, D., Savio, G., 2010. Slope failure and related processes in the Mt. Rocciamelone area (Cenischia Valley, Western Italian Alps). Geomorphology 114, 115–128. https://doi.org/10.1016/j.geomorph.2009.06.012.

Turconi, L., Nigrelli, G., Conte, R., 2014. Historical datum as a basis for a new GIS application to support civil protection services in NW Italy. Comput. Geosci. 66, 13–19. https://doi.org/10.1016/J.CAGEO.2013.12.008.

Van Der Schrier, G., Van Den Besselaar, E.J.M., Klein Tank, A.M.G., Verver, G., 2013. Monitoring European average temperature based on the E-OBS gridded data set. J. Geophys. Res. Atmos. 118, 5120–5135. https://doi.org/10.1002/jgrd.50444.

Velikou, K., Lazoglou, G., Tolika, K., Anagnostopoulou, C., 2022. Reliability of the ERA5 in replicating mean and extreme temperatures across Europe. Water (Switzerland) 14. https://doi.org/10.3390/w14040543.

Viani, C., Chiarle, M., Paranunzio, R., Merlone, A., Musacchio, C., Coppa, G., Nigrelli, G., 2020. An integrated approach to investigate climate-driven rockfall occurrence in high alpine slopes: the Bessanese glacial basin, Western Italian Alps. J. Mt. Sci. 17, 2591–2610. https://doi.org/10.1007/s11629-020-6216-y.

Villarini, G., Mandapaka, P.V., Krajewski, W.F., Moore, R.J., 2008. Rainfall and sampling uncertainties: a rain gauge perspective. J. Geophys. Res. Atmos. 113, 1–12. https://doi.org/10.1029/2007JD009214.

Zhou, H., Ning, S., Li, D., Pan, X., Li, Q., Zhao, M., Tang, X., 2023. Assessing the Applicability of three Precipitation Products, IMERG, GSMaP, and ERA5, in China over the last two decades. Remote Sens. 15 https://doi.org/10.3390/rs15174154.